

Neurofuzzy Model-Based Predictive Control of Weld Fusion Zone Geometry

Yu M. Zhang, *Senior Member, IEEE*, and Radovan Kovacevic

Abstract—A closed-loop system is developed to control the weld fusion, which is specified by the top-side and back-side bead widths of the weld pool. Because in many applications only a top-side sensor is allowed, which is attached to and moves with the welding torch, an image processing algorithm and neurofuzzy model have been incorporated to measure and estimate the top-side and back-side bead widths based on an advanced top-side vision sensor. The welding current and speed are selected as the control variables. It is found that the correlation between any output and input depends on the value of another input. This cross coupling implies that a nonlinearity exists in the process being controlled. A neurofuzzy model is used to model this nonlinear dynamic process. Based on the dynamic fuzzy model, a predictive control system has been developed to control the welding process. Experiments confirmed that the developed control system is effective in achieving the desired fusion state despite the different disturbances.

Index Terms— Fuzzy control, modeling, predictive control, welding.

I. INTRODUCTION

FUSION is the primary requirement of a welding operation. The fusion state can be specified using the outline of the cross-sectional solidified weld bead (Fig. 1). Extraction and control of the fusion outline is evidently impractical. A few geometrical parameters should be used to characterize the fusion zone and then be controlled to achieve the desired fusion.

This study focuses on controlling the fusion state of fully penetrated welds in gas tungsten arc (GTA) welding. The fusion state on a cross section is characterized using two parameters of the fusion zone, the top-side and back-side widths of the fusion zone (Fig. 1). Therefore, the top-side width w and back-side bead width w_b of the weld pool are referred to as the fusion state. A multivariable system will be developed to control w and w_b in this study.

Pool width control has been extensively studied. One of the pioneering works was done by Vroman and Brandt [1] who used a line scanner to detect the weld pool region. Chin *et al.* [2], [3] found that the slope of the infrared intensity

Manuscript received July 26, 1996; revised October 28, 1997. This work was supported by the National Science Foundation under Contract DMI-9634735, the Allison Engine Company, Indianapolis, IN, and the Center for Robotics and Manufacturing Systems, University of Kentucky, Lexington, KY.

Y. M. Zhang is with the Welding Research and Development Laboratory, Center for Robotics and Manufacturing Systems, University of Kentucky, Lexington, KY 40506 USA.

R. Kovacevic is with the Department of Mechanical Engineering, Southern Methodist University, Dallas, TX 75275 USA.

Publisher Item Identifier S 1063-6706(98)05151-0.

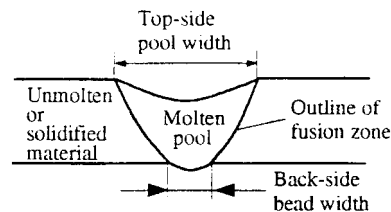


Fig. 1. Fusion parameters of fully penetrated weld pool.

becomes zero when the liquid-solid interface of the weld pool is crossed. This zero slope is caused by the emissivity difference between the liquid and solid [2]. In order to directly observe the weld pool, the intensive arc light should be avoided or eliminated. Richardson *et al.* [4] proposed the co-axial observation to avoid the arc light. Pietrzak and Packer [5] have developed a weld pool width control system based on the co-axial observation.

Compared with the pool width, weld penetration is a more critical component of the weld quality. For the case of full penetration, the state of the weld penetration is specified by the back-side bead width w_b (Fig. 1). With a back-side sensor, w_b can be reliably measured. However, it is often required that the sensor be attached to and move with the torch to form a so-called top-side sensor. For such a sensor, w_b is invisible. Hence, extensive studies have been done to explore the possibility of indirectly measuring w_b based on pool oscillation, infrared radiation, ultrasound, and radiography. Although many valuable results have been achieved, only a few control systems are available to quantitatively estimate and control the back-side bead width.

Fusion control requires the simultaneous control of both the top-side and back-side bead widths and is, therefore, more complicated than either penetration or pool width control. Hardt *et al.* [6] have simultaneously controlled the depth, which specifies the weld penetration state for the case of partial penetration and width of the weld pool using top-side and back-side sensors. To obtain a top-side sensor based control system, we have proposed estimating the back-side bead width using the sag geometry behind the weld pool [7]. Based on a detailed dynamic modeling study [8], an adaptive system has been developed to control both the top-side and back-side widths of the weld pool [9]. In this case, a delay arises since the feedback can only be measured at the already solidified sag behind the pool.

More instantaneous and accurate information can be acquired from the weld pool. In order to use the weld pool information in welding process control, a real-time image

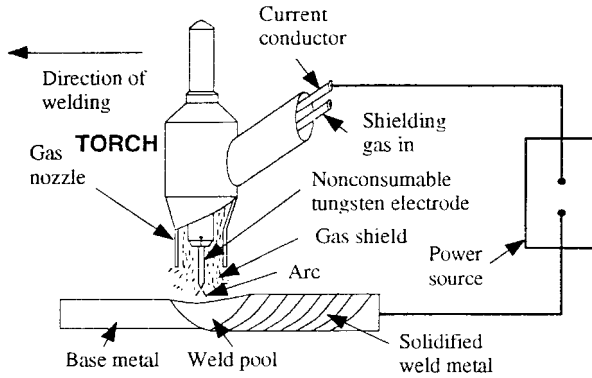


Fig. 2. GTA welding.

processing algorithm was developed to detect the weld pool boundary in a previous study [10] from the images captured by a high-shutter-speed camera assisted with a pulsed laser [11]. Hence, the weld pool geometry can be utilized to develop more advanced welding process control systems.

It is known that skilled operators can estimate and control the welding process based on pool observation. This implies that an advanced control system could be developed to control the fusion state by emulating the estimation and decision making processes of human operators. In the past, operator's experience was the major source to establish the fuzzy model that emulates the operator. Recently, neurofuzzy approach, i.e., determining the parameters in fuzzy models using optimization algorithms developed in neural network training, has been employed to establish fuzzy models based on experimental data. Hence, we developed a neurofuzzy system for estimating the back-side bead width from the pool geometry [12]. In this work, a neurofuzzy dynamic model based multivariable system will be designed to control the fusion state using the top-side pool width and the estimated back-side bead width as the feedback of the fusion state.

II. PROCESS

A. Controlled Process

GTA is used for precise joining of metals. The GTA welding process is illustrated in Fig. 2. A nonconsumable tungsten electrode is held by the torch. Once the arc is established, the electrical current flows from one terminal of the power supply to another terminal through the electrode, arc and workpiece. The temperature of the arc can reach 8000–10 500 K [13] and, therefore, the workpiece becomes molten forming the weld pool, whereas the tungsten electrode remains unmolten. The shielding gas is fed through the torch to protect the electrode, molten weld pool, and solidifying weld metal from being contaminated by the atmosphere.

The major adjustable welding parameters include the welding current, arc length, and travel speed of the torch. In general, the weld pool increases as the current increases and the travel speed decreases. For GTA welding, the welding current is maintained constant by the inner closed-loop control system of the power supply despite the variations in the arc length and other parameters. Thus, when the arc length

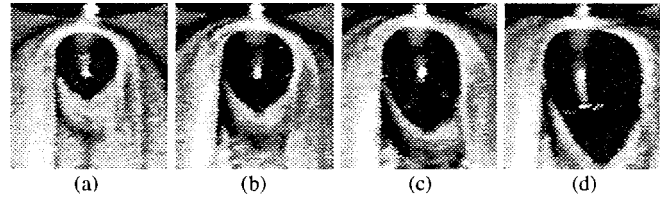


Fig. 3. Weld pools made using different welding speeds. Current: 100 A; arc length: 3 mm, 3 mm 304 stainless steel. (a) 2.92 mm/s. (b) 2.42 mm/s. (c) 1.95 mm/s. (d) 1.43 mm/s.

increases, the arc voltage increases so that the arc power increases, but the distribution of the arc energy is decentralized so that the efficiency of the arc decreases. As a result, the correlation between the weld pool and arc length may not be straightforward. In addition to these three welding parameters, the weld pool is also determined by the welding conditions such as the heat transfer condition, material, thickness, and chemical composition of the workpiece, shielding gas, angle of the electrode tip, etc. In a particular welding process control system, only a few selected welding parameters are adjusted through the feedback algorithm to compensate for the variations in the welding conditions.

Compared with the arc length, the roles of the welding current and welding speed in determining the weld pool and weld fusion geometry are much more significant and definite. For many automated welding systems, the welding speed can be adjusted on-line. Such an on-line adjustment may also be done for many advanced welding robots with proper interfaces. Thus, in addition to the welding current, we selected the welding speed as another control variable. The controlled process can therefore be defined as a GTA welding process in which the welding current and speed are adjusted on-line to achieve the desired back-side and top-side widths of the weld pool.

B. Nonlinearity

The heat input of the arc in a unit interval along the travel direction can be written as

$$\Delta H \propto (i^2/v)u \quad (1)$$

where i is the welding current, v is the welding speed, and u is the welding voltage. Roughly speaking, one can assume that the area of the weld pool is approximately proportional to ΔH .

When the welding speed changes, both the length L and width w of the weld pool alter. However, their ratio w/L , referred to as the relative width of the weld pool in this work, does not change significantly (ranged from 0.72 to 0.85 in Fig. 3). This suggests that

$$\begin{aligned} L &\propto (i\sqrt{u})(1/\sqrt{v}) \\ w &\propto (i\sqrt{u})(1/\sqrt{v}) \end{aligned}$$

In our case, the voltage u can be assumed constant. Hence,

$$\begin{aligned} L &\propto f_1(i)(1/\sqrt{v}) \\ w &\propto f_1(i)(1/\sqrt{v}) \end{aligned} \quad (2)$$

where $f_1(i) = i\sqrt{u}$.

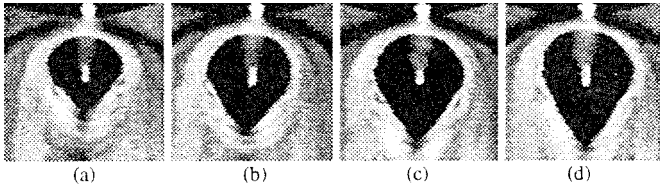


Fig. 4. Weld pools made using different currents. Arc length: 3 mm; speed: 1.9 mm/s, 3 mm 304 stainless steel. (a) 95 A. (b) 105 A. (c) 110 A. (d) 115 A.

When the current increases, the relative width w/L decreases (Fig. 4). This implies

$$\begin{aligned} L &\propto (f_2(v))^{c_1} i^{c_1} \\ w &\propto (f_2(v))^{c_2} i^{c_2} \end{aligned} \quad (3)$$

where $c_1 > 1, 0 < c_2 < 1, c_1 + c_2 = 2$, and $f_2(v) = \sqrt{u/v}$.

During closed-loop control, the control variables i and v are subject to fundamental adjustments so that f_1 and f_2 change as the control variables move in the control variable plan $i \sim v$. Hence, the correlation between the top-side geometrical parameters (width and length) of the weld pool and the input variables is nonlinear. Because of the correlation between the back-side bead width and the top-side geometrical parameters, it is apparent that the correlation between the back-side bead width and the control variables is also nonlinear. Hence, the controlled plant is a two-input–two-output nonlinear multivariable process. Because of the thermal inertia, the process will also be dynamic.

III. NEUROFUZZY NONLINEAR DYNAMIC MODELING

A. Neurofuzzy Modeling

A fuzzy system has three major conceptual components: rule base, database, and reasoning mechanism [14]. The rule base consists of the used fuzzy IF–THEN rules. The database contains the membership functions of the fuzzy sets. The reasoning mechanism performs the inference procedure for deriving a reasonable output or conclusion based on the IF–THEN rules from the input variables.

In the conventional fuzzy models, the fuzzy linguistic IF–THEN rules are primarily derived from human experience [15]. Because the fuzzy modeling takes advantage of existing human knowledge, which might not be easily or directly utilized by other conventional modeling methods [14], such fuzzy models have been successfully used in different areas, including manufacturing [16]–[19]. In these models, no systematic adjustments are made on the used rules, membership functions, or reasoning mechanism based on the behavior of the fuzzy model. In general, if the fuzzy rules elicited from the operators' experience are correct, relevant, and complete [20], the resultant fuzzy model can function well. However, frequently such fuzzy rules from the operators do not satisfy the correctness, relevance, and completeness requirements [20]; the rules may be vague and misinterpreted, or the rule base could be incomplete. In such cases, the performance of the fuzzy system can be greatly improved if systematic adjustments are made based on its behavior.

The adjustability of the used rules, membership functions, and reasoning mechanism allow the fuzzy model to adapt to the addressed problem or process. In order to adjust the parameters in the fuzzy model, various learning techniques developed in the neural network literature have been used. Thus, the term neurofuzzy modeling is used to refer to the application of algorithms developed through neural network training to identify parameters for a fuzzy model [14]. A neurofuzzy model can be defined as a fuzzy model with parameters, which can be systematically adjusted using the training algorithms in neural network literature. In neurofuzzy modeling, the abstract thoughts or concepts in human reasoning are combined with numerical data so that the development of fuzzy models becomes more systematic and less time consuming. As a result, neurofuzzy systems have been successfully used in different areas [21]–[24].

Most neurofuzzy systems have been developed based on the Sugeno-type fuzzy model [25]. A typical fuzzy rule in a Sugeno-type model has the form: IF x is A and y is B THEN $z = f(x, y)$. Here, A and B are fuzzy sets and $z = f(x, y)$ is a crisp function which can be any function as long as the system outputs can be appropriately described within the fuzzy region specified by the antecedent of the rule [14]. In this paper, a neurofuzzy system will be developed to model the nonlinear dynamics of the process being controlled.

B. Model

Relationships in (2) and (3) imply that the fuzzy model can be established based on partitioning the inputs. Define $y_1 = w_b$ and $y_2 = w$ as the outputs, $u_1 = i$ and $u_2 = 1/v$ as the control variables. In this study, the units of u_1 and u_2 are 100 A and 1/mm, respectively. Denote the present time instant by t . Consider the following model:

$$\begin{aligned} y_1(t) &= \sum_{j=1}^{n_{11}} c_{11}(j)u_1(t-j) + \sum_{j=1}^{n_{12}} c_{12}(j)u_2(t-j) \\ y_2(t) &= \sum_{j=1}^{n_{21}} c_{21}(j)u_1(t-j) + \sum_{j=1}^{n_{22}} c_{22}(j)u_2(t-j) \end{aligned} \quad (4)$$

where $c_{k_1 k_2}(j)$'s and $n_{k_1 k_2}$'s ($k_1 = 1, 2; k_2 = 1, 2; j = 1, \dots, n_{k_1 k_2}$) are the parameters and orders of the model. This is an impulse response function that is widely used in industrial processes. If the model parameters $c_{k_1 k_2}(j)$'s are constant for each given (k_1, k_2, j) , (4) will be a linear time-invariant model. If the parameters are dependent on t , the model will be linear time-varying. In our case, due to the cross-coupling, $c_{11}(j)$'s and $c_{21}(j)$'s will depend on u_2 , and $c_{12}(j)$'s and $c_{22}(j)$'s on u_1 . The model is nonlinear.

In order to model the nonlinear welding process, the control variables are first partitioned into a number of fuzzy sets. (Modeling comparison shows that the partition of four sets shown in Table I is optimal for both variables.) For the welding current, the four fuzzy sets are low, middle, high, and very high. For $u_2 = 1/v$, the four fuzzy sets are: small, moderate, large, and very large. For a given value of u_j , the degree of truth that u_j belongs to its i th fuzzy set is measured by the

TABLE I
FUZZY PARTITION OF CONTROL VARIABLES

Fuzzy variables	Number of fuzzy sets	Partition
u_1	$I_1 = 4$	low (A_{11}), middle (A_{12}), high (A_{13}), very high (A_{14})
u_2	$I_2 = 4$	small (A_{21}), moderate (A_{22}), large (A_{23}), very large (A_{24})

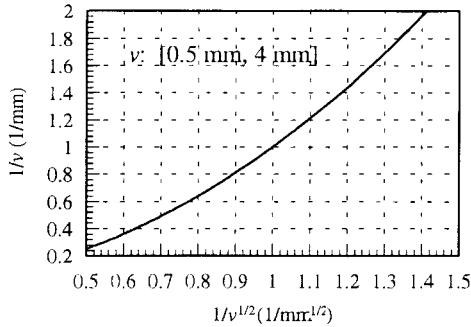


Fig. 5. $1/\sqrt{v} \sim 1/v$.

membership function A_{ji}

$$A_{ji}(u_j) = \exp(-(u_j - a_{ji})^2/b_{ji}) \quad (1 \leq i \leq I_j) \quad (5)$$

where I_j is the number of the partitioned fuzzy sets for u_j ($j = 1, 2$), a_{ji} and b_{ji} are the parameters of the membership function.

Based on the partition of the control variables, the following rules can be applied:

$$\begin{aligned} \text{If } u_2(t-j) \text{ is } A_{2i_2} \text{ then } c_{k1}(j) &= c_{k1}(j/i_2) \\ \text{If } u_1(t-j) \text{ is } A_{1i_1} \text{ then } c_{k2}(j) &= c_{k2}(j/i_1) \quad (k = 1, 2). \end{aligned} \quad (6a)$$

Here, $c_{k1}(j/i_2)$ and $c_{k2}(j/i_1)$ are constant for the given j , i_1 , and i_2 . Also, i_2 in $c_{k1}(j/i_2)$ and i_1 in $c_{k2}(j/i_1)$ are used to indicate that the parameters $c_{k1}(j)$ and $c_{k2}(j)$ [in model (4)] depend on the partition set i_2 and i_1 to which $u_2(t-j)$ and $u_1(t-j)$ belong, respectively.

Rule (6a) is designed to account for the cross-coupling only. Theoretically, based on (2) and (3), the rule should be:

$$\begin{aligned} \text{If } u_1(t-j) \text{ is } A_{1i_1} \text{ and } u_2(t-j) \text{ is } A_{2i_2} \text{ then} \\ c_{k1}(j) = c_{k1}(j/i_1, i_2) \text{ and } c_{k2}(j) = c_{k2}(j/i_1, i_2). \end{aligned} \quad (6b)$$

However, in our case, the range of the welding speed in the closed-loop control will be 1.0–3.0 mm. In this range, the correlation between $1/\sqrt{v}$ and $1/v$ can be roughly linear (Fig. 5). Hence, we can regard $L \propto f_1(i)(1/v)$ and $w \propto f_1(i)(1/v)$. Also, from Fig. 4, the static correlations between the weld pool parameters and the welding current in Fig. 6 can be obtained. Again, although the correlations are nonlinear, the nonlinearity is slight. As a result, as will be discussed in Section V, experimental data analysis suggests that the above more complex rule (6b) does not significantly improve the modeling. This implies that the cross-coupling is the dominant factor which causes the nonlinearity. Hence, (6a) is used.

In our case, the partition is fuzzy. This implies that $u_2(t-j)$ (or $u_1(t-j)$) may simultaneously belong to A_{21} , \dots , and A_{2I_2} (or A_{11} , \dots , and A_{1I_1}), but with different membership functions. Hence

$$\begin{aligned} c_{k1}(j) &= \sum_{i_2=1}^{I_2} A_{2i_2}(u_2(t-j))c_{k1}(j/i_2) \\ &\quad (k = 1, 2; j = 1, \dots, n_{k1}) \\ c_{k2}(j) &= \sum_{i_1=1}^{I_1} A_{1i_1}(u_1(t-j))c_{k2}(j/i_1) \\ &\quad (k = 1, 2; j = 1, \dots, n_{k2}). \end{aligned} \quad (7)$$

IV. IDENTIFICATION ALGORITHM

The identification of a fuzzy model consists of structure identification and parameter estimation. During identification, the parameters are estimated for different structures. The final structure, i.e., the fuzzy variable partition in this case, is selected by comparing different models. This is, in general, very inefficient. Also, the decision is made purely based on statistical (mathematical) analysis. No process characteristics or designer's experience are involved. If the designer is familiar with the process, an experience-based partition may be appropriate. Thus, as suggested in [14], we have selected and partitioned the fuzzy variables based on our understanding of the welding process (Table I). Hence, the identification of the fuzzy model is simplified as a parameter estimation problem.

Denote the data as

$$\{u_1(t), u_2(t), y_1(t), y_2(t)\} \quad (T_0 \leq t \leq T_1) \quad (8)$$

and the prediction errors as

$$\begin{aligned} \delta_1(t) &:= y_1(t) - \hat{y}_1(t) \\ \delta_2(t) &:= y_2(t) - \hat{y}_2(t). \end{aligned} \quad (9)$$

Define the cost function

$$\begin{aligned} J\{(a_{ji}, b_{ji})'s \ (1 \leq i \leq I_j, 1 \leq j \leq 2); c_{k1}(j/i_2)'s \\ (k = 1, 2; 1 \leq i_2 \leq I_2; j = 1, \dots, n_{k1}); c_{k2}(j/i_1)'s \\ (k = 1, 2; 1 \leq i_1 \leq I_1; j = 1, \dots, n_{k2}) \\ = \sum_{t=T_0}^{T_1} \{(y_1(t) - \hat{y}_1(t))^2 + (y_2(t) - \hat{y}_2(t))^2\}. \end{aligned} \quad (10)$$

The parameter estimation is to find the optimal parameters $\{(a_{ji}^*, b_{ji}^*)'s, c_{k1}^*(j/i_2)'s, c_{k2}^*(j/i_1)'s\}$ so that

$$\begin{aligned} J\{(a_{ji}^*, b_{ji}^*)'s, c_{k1}^*(j/i_2)'s, c_{k2}^*(j/i_1)'s\} \\ = \min J\{(a_{ji}, b_{ji})'s, c_{k1}(j/i_2)'s, c_{k2}(j/i_1)'s\}. \end{aligned} \quad (11)$$

Although many excellent algorithms such as the second-order back-propagation [26] and normalized cumulative learning rule [27] proposed in the neural network literature can be used to speed up the parameter identification, the authors found that satisfactory identification speed can be achieved by using the simplest, but the most frequently used δ rule [27], [28] in this case. In order to implement this algorithm, partial derivatives of the cost function with respect to each of the

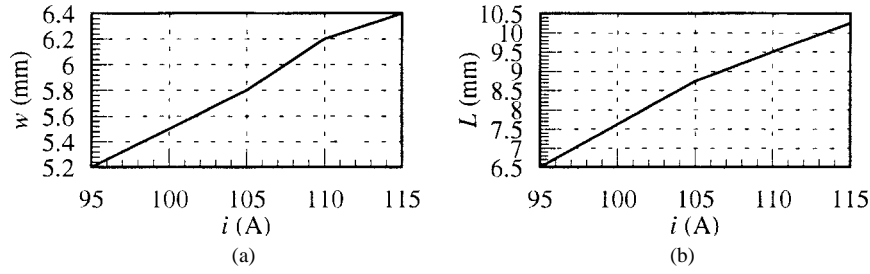


Fig. 6. Empirical static correlations between the welding current and weld pool parameters. (a) $L \sim i$. (b) $w \sim i$. The experimental data in Fig. 4 are used.

model parameters are needed. The following can be shown:

$$\begin{aligned} \frac{\partial J}{\partial a_{1i}} &= -2 \sum_{t=T_0}^{T_1} \left\{ \delta_1(t) \frac{\partial \hat{y}_1(t)}{\partial a_{1i}} + \delta_2(t) \frac{\partial \hat{y}_2(t)}{\partial a_{1i}} \right\} \\ &= -2 \sum_{t=T_0}^{T_1} \left\{ \delta_1(t) \sum_{j=1}^{n_{12}} u_2(t-j) \frac{\partial c_{12}(j)}{\partial a_{1i}} \right. \\ &\quad \left. + \delta_2(t) \sum_{j=1}^{n_{22}} u_2(t-j) \frac{\partial c_{22}(j)}{\partial a_{1i}} \right\} \\ &= -4 \sum_{t=T_0}^{T_1} \left\{ \delta_1(t) \sum_{j=1}^{n_{12}} u_2(t-j) c_{12}(j/i) A_{1i}(u_1(t-j)) \right. \\ &\quad \cdot \frac{u_1(t-j) - a_{1i}}{b_{1i}} \\ &\quad \left. + \delta_2(t) \sum_{j=1}^{n_{22}} u_2(t-j) c_{22}(j/i) A_{1i}(u_1(t-j)) \right. \\ &\quad \left. \cdot \frac{u_1(t-j) - a_{1i}}{b_{1i}} \right\} \end{aligned} \quad (i = 1, \dots, I_1) \quad (12)$$

$$\begin{aligned} \frac{\partial J}{\partial a_{2i}} &= -4 \sum_{t=T_0}^{T_1} \left\{ \delta_1(t) \sum_{j=1}^{n_{11}} u_1(t-j) c_{11}(j/i) A_{2i}(u_2(t-j)) \right. \\ &\quad \cdot \frac{u_2(t-j) - a_{2i}}{b_{2i}} \\ &\quad \left. + \delta_2(t) \sum_{j=1}^{n_{21}} u_1(t-j) c_{21}(j/i) A_{2i}(u_2(t-j)) \right. \\ &\quad \left. \cdot \frac{u_2(t-j) - a_{2i}}{b_{2i}} \right\} \quad (i = 1, \dots, I_2) \quad (13) \end{aligned}$$

$$\begin{aligned} \frac{\partial J}{\partial b_{1i}} &= -2 \sum_{t=T_0}^{T_1} \left\{ \delta_1(t) \sum_{j=1}^{n_{12}} u_2(t-j) c_{12}(j/i) A_{1i}(u_1(t-j)) \right. \\ &\quad \cdot \frac{(u_1(t-j) - a_{1i})^2}{b_{1i}^2} \\ &\quad \left. + \delta_2(t) \sum_{j=1}^{n_{22}} u_2(t-j) c_{22}(j/i) A_{1i}(u_1(t-j)) \right. \\ &\quad \left. \cdot \frac{(u_1(t-j) - a_{1i})^2}{b_{1i}^2} \right\} \quad (i = 1, \dots, I_1) \quad (14) \end{aligned}$$

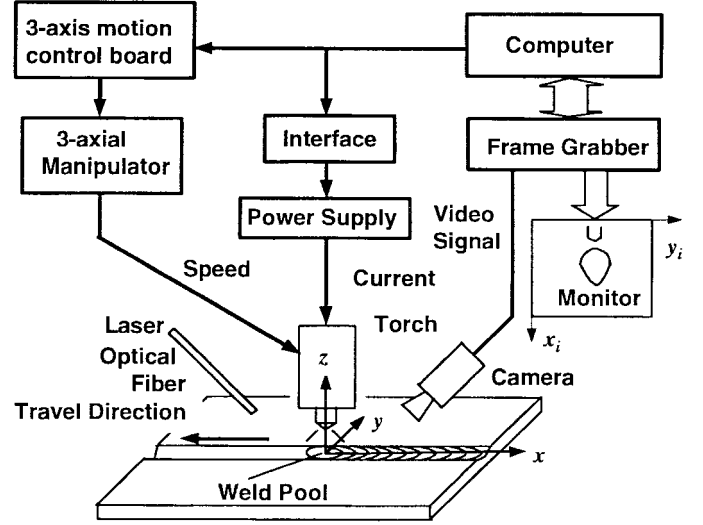


Fig. 7. Experimental setup.

$$\begin{aligned} \frac{\partial J}{\partial b_{2i}} &= -2 \sum_{t=T_0}^{T_1} \left\{ \delta_1(t) \sum_{j=1}^{n_{11}} u_1(t-j) c_{11}(j/i) A_{2i}(u_2(t-j)) \right. \\ &\quad \cdot \frac{u_2(t-j) - a_{2i}}{b_{2i}^2} \\ &\quad \left. + \delta_2(t) \sum_{j=1}^{n_{21}} u_1(t-j) c_{21}(j/i) A_{2i}(u_2(t-j)) \right. \\ &\quad \left. \cdot \frac{u_2(t-j) - a_{2i}}{b_{2i}^2} \right\} \quad (i = 1, \dots, I_2) \quad (15) \end{aligned}$$

$$\begin{aligned} \frac{\partial J}{\partial c_{k1}(j/i_2)} &= -2 \sum_{t=T_0}^{T_1} \delta_k(t) \frac{\partial \hat{y}_k(t)}{\partial c_{k1}(j/i_2)} \\ &= -2 \sum_{t=T_0}^{T_1} \delta_k(t) u_1(t-j) \frac{\partial c_{k1}(j)}{\partial c_{k1}(j/i_2)} \\ &= -2 \sum_{t=T_0}^{T_1} \delta_k(t) u_1(t-j) A_{2i_2}(u_2(t-j)) \end{aligned} \quad (k = 1, 2; j = 1, \dots, n_{k1}; i_2 = 1, \dots, I_2) \quad (16)$$

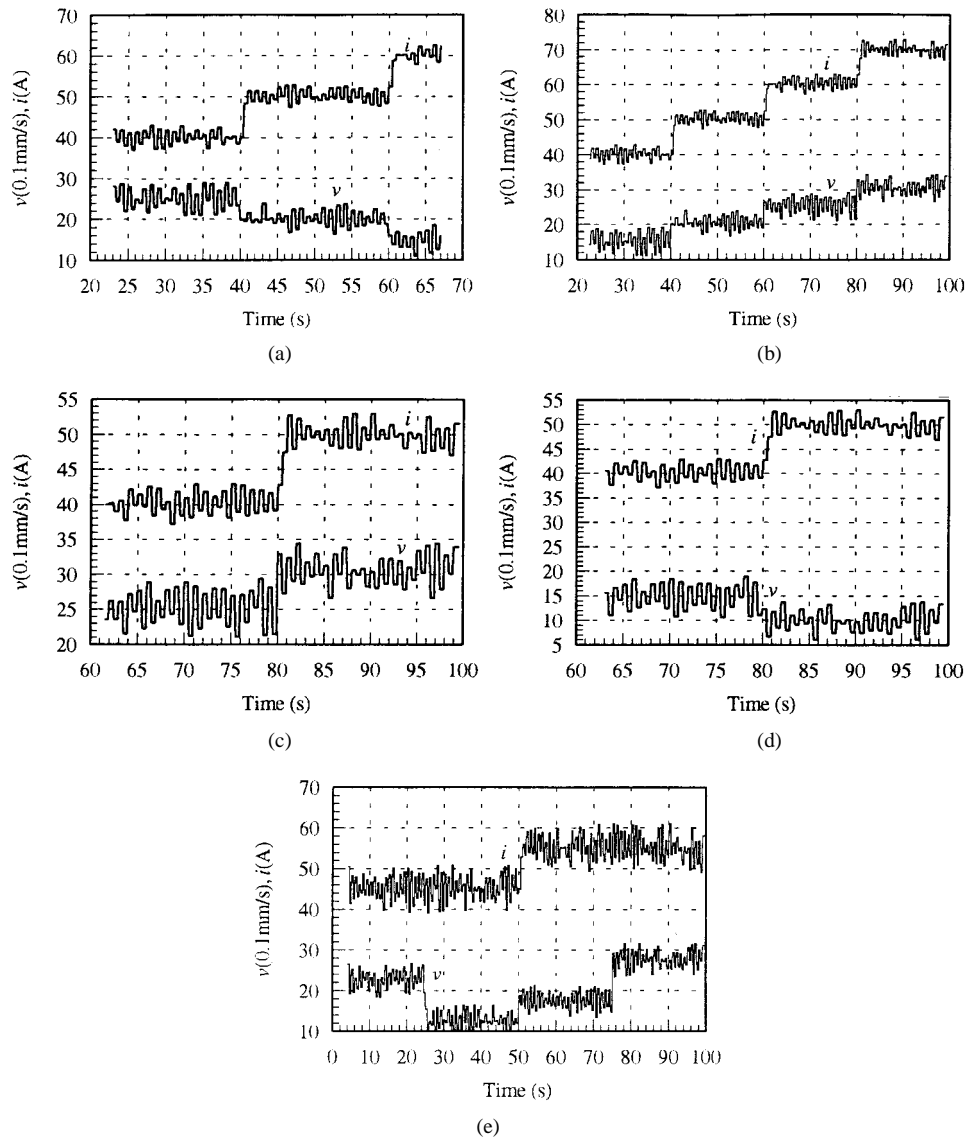


Fig. 8. Inputted welding parameters for the five dynamic experiments.

$$\frac{\partial J}{\partial c_{k2}(j/i_1)} = -2 \sum_{t=T_0}^{T_1} \delta_k(t) u_2(t-j) A_{1i_2}(u_1(t-j))$$

$$(k = 1, 2; j = 1, \dots, n_{k2}; i_1 = 1, \dots, I_1).$$
(17)

Thus, an identification procedure can be designed accordingly.

V. DYNAMIC EXPERIMENTS

The experimental setup is shown in Fig. 7. The welds are made using direct-current GTA welding with the electrode negative [13]. The welding current is controlled by the computer through its analog output to the power supply ranging from 10 to 200 A. The torch and camera are attached to a three-axial manipulator. The motion of the manipulator is controlled by the three-axis motion control board, which receives the commands from the computer. The motion can be preprogrammed and on-line modified by the computer in order to achieve the required torch speed and trajectory, including the arc length. The control vision's ultrahigh-shutter-speed

vision system [11] is used to capture the weld pool images. This system consists of a strobe-illumination unit (pulse laser), camera head, and system controller. The pulse duration of the laser is 3 ns and the camera is synchronized with the laser pulse. Thus, the intensity of laser illumination during the pulse duration is much higher than those of the arc and hot metal. Using this vision system, good weld pool contrast can always be obtained under different welding conditions. In this study, the camera views the weld pool from the rear at a 45° angle. The frame grabber digitizes the video signals into 512 × 512 8 bit digital image matrices. By improving the algorithm [10] and hardware, the weld pool boundary can now be acquired on-line in 80 ms.

Five experiments have been done on 1-mm-thick stainless steel 304 plates. The workpieces are 250 mm in length and 100 mm in width. The shielding gas is pure argon. The arc length is 3 mm in all the experiments. In order to establish the full penetration mode, the current and welding speed must be in certain ranges. We have used control variables in larger ranges. Fig. 8 plots the segments in each experiment where

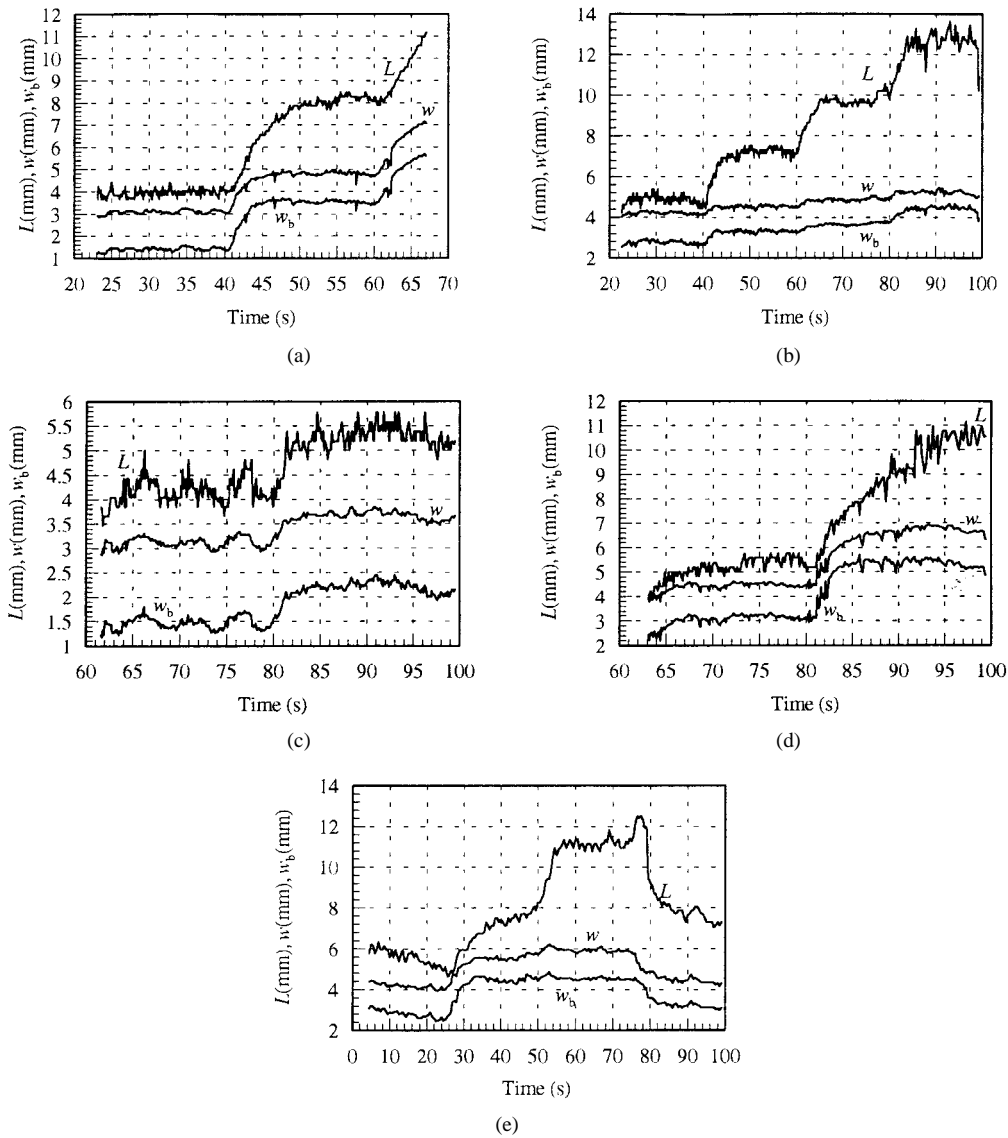


Fig. 9. Measured pool parameters from the five dynamic experiments.

the inputs have produced fully penetrated weld pools. The measured parameters of the weld pools in these segments are given in Fig. 9. The back-side bead width can be calculated using the weld pool parameters and the neurofuzzy model developed in the previous study [12]. The results have also been illustrated in Fig. 9.

Fig. 10 shows the distribution of the control variables in these segments of experiments. It can be seen that the welding parameters have filled the projected range of the control variables. This distribution implies that the resultant model can be used during control if the control variables are in the projected range.

The above experimental data have been used to fit a neurofuzzy model here. It is found that orders $n_{11} = n_{12} = n_{21} = n_{22} = 4$ are sufficient when the sample period $T = 1$ s. The identified model parameters are given in Tables II–VI. Here $u_1(t - j)$ and $u_2(t - j)$ are the average inputs in $[(t - j)T - 0.5T, (t - j)T + 0.5T]$, rather than at discrete instant $t - j$.

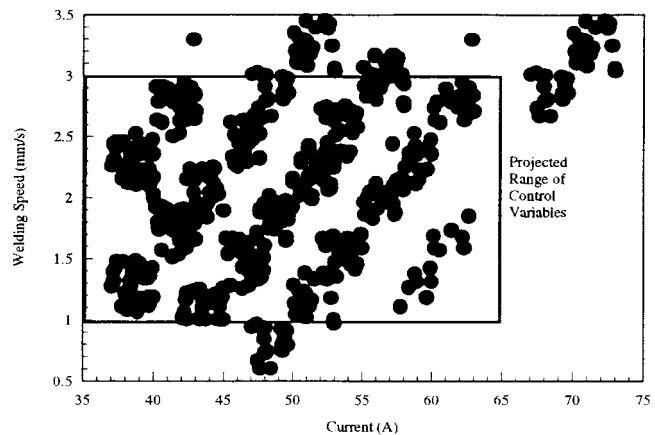


Fig. 10. Distribution of inputs in the dynamic experiments.

Assume that τ represents the continuous time rather than the discrete-time instant. The outputs at τ can be predicted using the inputs in $(\tau - jT - 0.5T, \tau - jT + 0.5T]$'s ($j = 1, \dots, \max(n_{11}, \dots, n_{22})$) no matter whether or not τ/T is an

TABLE II
IDENTIFIED FUZZY PARTITION PARAMETERS

	$k=1$	$k=2$	$k=3$	$k=4$
a_{1k}	0.30	0.43	0.56	0.7
a_{2k}	0.30	0.53	0.76	1.0
$b_{1k} (\times 0.001)$	8.45	8.45	8.45	8.45
$b_{2k} (\times 0.01)$	2.64	2.64	2.64	2.64

TABLE III
IDENTIFIED $c_{11}(j/i_2)$'s

	$i_2=1$	$i_2=2$	$i_2=3$	$i_2=4$
$j=1$	2.54	1.50	1.42	.85
$j=2$.096	.36	.46	.37
$j=3$	1.96	1.64	1.27	0.54
$j=4$	-3.04	-1.68	-0.12	-0.40

TABLE IV
IDENTIFIED $c_{12}(j/i_1)$'s

	$i_1=1$	$i_1=2$	$i_1=3$	$i_1=4$
$j=1$	-0.10	1.42	1.95	1.66
$j=2$	-1.01	.723	.850	2.29
$j=3$.078	1.38	1.43	0.92
$j=4$	-2.08	-0.47	-0.11	3.9

TABLE V
IDENTIFIED $c_{21}(j/i_2)$'s

	$i_2=1$	$i_2=2$	$i_2=3$	$i_2=4$
$j=1$	3.45	2.75	2.16	.711
$j=2$.703	.875	.614	-0.03
$j=3$.712	.444	.382	-0.22
$j=4$	-1.90	-1.54	-0.41	-0.56

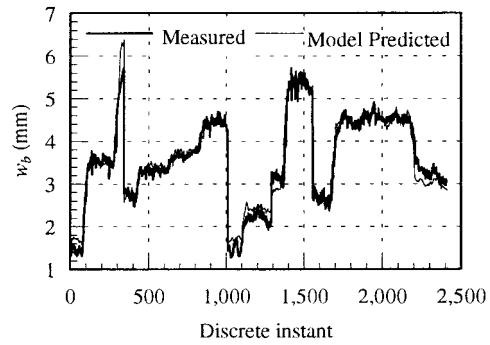
TABLE VI
IDENTIFIED $c_{22}(j/i_1)$'s

	$i_1=1$	$i_1=2$	$i_1=3$	$i_1=4$
$j=1$	1.48	2.06	2.49	2.28
$j=2$.703	1.21	1.54	2.73
$j=3$.207	.933	1.35	.950
$j=4$	-1.48	-0.04	.373	1.96

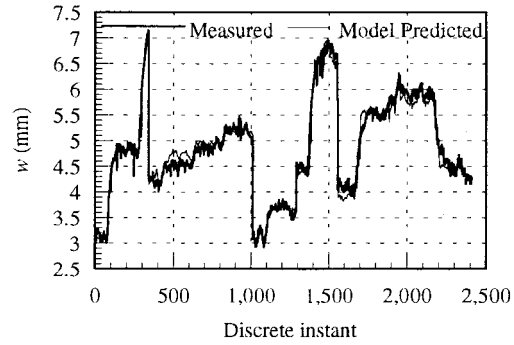
integer. Hence, by applying the identified model, the outputs at any moment can be predicted.

The modeling accuracy of the resultant fuzzy model can be seen in Fig. 11 where the outputs were measured at 10 Hz. The variances of the fitting errors are 0.039 and 0.020 mm² for w and w_b , respectively. It is found that the no noticed improvement can be made when increasing $n_{k_1 k_2}$'s, increasing I_1 and I_2 , or using (6b). In fact, the welding process is subject to uncertainty and its outputs cannot be exactly predicted using the inputs without any errors. The prediction errors in Fig. 11 are certainly not larger than the deviations of the outputs caused by the uncontrollable variations in the welding process when the same inputs are used. Hence, the obtained model is sufficient.

In order to show the effectiveness of the fuzzy model, a linear model has also been fitted. It is found that the modeling is much poorer (Fig. 12). It is apparent that the



(a)



(b)

Fig. 11. Neurofuzzy modeling results. (a) Back-side bead width y_1 . (b) Top-side bead width y_2 .

used neurofuzzy model structure has played a critical role in accurately modeling the nonlinear dynamics of the process being controlled.

VI. FUZZY MODEL-BASED PREDICTIVE CONTROL

A number of methods could be used to design a neurofuzzy controller [14], including mimicking another working controller, inverse model, specialized learning, back-propagation through time and real-time recurrent learning, feedback linearization and sliding control, gain scheduling, etc. The advantage and limitation of each individual method has been analyzed in [14].

Traditionally, fuzzy controllers have been designed without an explicit model of the process being controlled. However, in neurofuzzy systems, mathematical models are explicitly used. We notice that the predictive control principle [29] has recently been incorporated with fuzzy models to provide design methods for neurofuzzy model based controllers because predictive methods have several advantages that make them good candidates for industrial applications. Oliveira and Lemos proposed a fuzzy model based predictive controller for single-input single-output systems [30]. They used relational fuzzy models, rather than the Sugeno-type models as used in our work. Next, we will develop a predictive controller for our two-input two-output Sugeno-type model.

At t , the controller needs to determine the control action $(u_1(t), u_2(t))$ based on the feedback $(y_1(t), y_2(t))$ to drive the welding process to reach the desired outputs (Y_{10}, Y_{20}) . In a predictive control, prediction equations should be developed to predict the outputs. Equation (4) can directly yield the

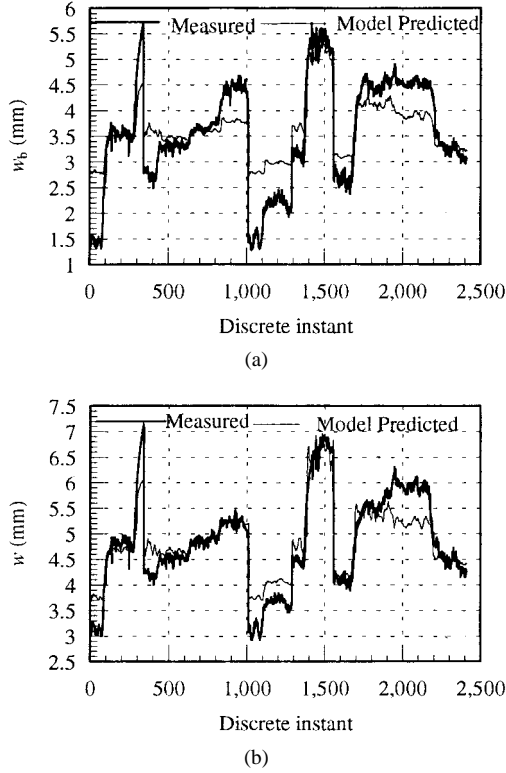


Fig. 12. Linear modeling (without variable partition). (a) Back-side bead width y_1 . (b) Top-side bead width y_2 .

following recursive prediction equations:

$$\begin{aligned}
 & \hat{y}_1(t+k) \\
 &= \hat{y}_1(t+k-1) \\
 &+ \sum_{j=1}^{n_{11}} c_{11}(j, u_2(t+k-j)) u_1(t+k-j) \\
 &- \sum_{j=1}^{n_{11}} c_{11}(j, u_2(t+k-1-j)) u_1(t+k-1-j) \\
 &+ \sum_{j=1}^{n_{12}} c_{12}(j, u_1(t+k-j)) u_2(t+k-j) \\
 &- \sum_{j=1}^{n_{12}} c_{12}(j, u_1(t+k-1-j)) u_2(t+k-1-j) \\
 & \hat{y}_2(t+k) \\
 &= \hat{y}_2(t+k-1) \\
 &+ \sum_{j=1}^{n_{21}} c_{21}(j, u_2(t+k-j)) u_1(t+k-j) \\
 &- \sum_{j=1}^{n_{21}} c_{21}(j, u_2(t+k-1-j)) u_1(t+k-1-j) \\
 &+ \sum_{j=1}^{n_{22}} c_{22}(j, u_1(t+k-j)) u_2(t+k-j) \\
 &- \sum_{j=1}^{n_{22}} c_{22}(j, u_1(t+k-1-j)) u_2(t+k-1-j) \\
 & \quad (k \geq 1)
 \end{aligned} \tag{18}$$

with initials

$$\begin{aligned}
 \hat{y}_1(t) &= y_1(t) \\
 \hat{y}_2(t) &= y_2(t)
 \end{aligned} \tag{19}$$

where notations $c_{11}(j, u_2(t+k-j)), \dots$, emphasize that $c_{11}(j), \dots$, are dependent on $u_2(t+k-j), \dots$.

In order to achieve a robust control, it is required that the following cost function is minimized:

$$G = [\hat{y}_1(t+K) - Y_{10}]^2 + [\hat{y}_2(t+K) - Y_{20}]^2. \tag{20}$$

In a long-range predictive control, the positive integer K should be large enough in order to achieve a robust control. In general, the regulation speed increases when K decreases. However, the robustness of the closed-loop control system becomes poorer. For welding process control, the robustness is the primary requirement. It is found that $K = 4$ can achieve satisfactory regulation speed and excellent robustness.

It is known that fluctuations in welding parameters will generate nonsmooth weld appearance, which is not acceptable. Energetic control actions must be avoided. Although all of $u_1(t), \dots, u_1(t+K-1), u_2(t), \dots, u_2(t+K-1)$ can be free variables in optimizing the cost function G , only $u_1(t)$ and $u_2(t)$ will be actually applied. (In fact, at the succeeding instants, $u_1(t+1), \dots, u_2(t+1), \dots$ will be determined again.) In addition, being free variables, $u_1(t), \dots, u_1(t+K-1)$ and $u_2(t), \dots, u_2(t+K-1)$ could vary severely so that energetic control actions are generated. Hence, the outputs can be predicted to optimize the cost function by assuming constant control variables in the prediction horizon, i.e., $u_1(t+k) = u_1(t)$ and $u_2(t+k) = u_2(t)$ ($k \geq 1$). In this case, the prediction equations will be

$$\begin{aligned}
 \hat{y}_1(t+k) &= F_1(k) + A_{11}(k)u_1(t) + A_{12}(k)u_2(t) \\
 \hat{y}_2(t+k) &= F_2(k) + A_{21}(k)u_1(t) + A_{22}(k)u_2(t) \\
 & \quad (k \geq 1)
 \end{aligned} \tag{21}$$

where

$$\begin{aligned}
 F_1(k) &= F_1(k-1) + \sum_{j=k+1}^{n_{11}} c_{11}(j, u_2(t+k-j)) \\
 & \quad \cdot u_1(t+k-j) \\
 & \quad - \sum_{j=k}^{n_{11}} c_{11}(j, u_2(t+k-1-j)) u_1(t+k-1-j) \\
 & \quad + \sum_{j=k+1}^{n_{12}} c_{12}(j, u_1(t+k-j)) u_2(t+k-j) \\
 & \quad - \sum_{j=k}^{n_{12}} c_{12}(j, u_1(t+k-1-j)) u_2(t+k-1-j) \\
 F_2(k) &= F_2(k-1) + \sum_{j=k+1}^{n_{21}} c_{21}(j, u_2(t+k-j)) \\
 & \quad \cdot u_1(t+k-j) \\
 & \quad - \sum_{j=k}^{n_{21}} c_{21}(j, u_2(t+k-1-j)) u_1(t+k-1-j)
 \end{aligned}$$

$$\begin{aligned}
& + \sum_{j=k+1}^{n_{22}} c_{22}(j, u_1(t+k-j))u_2(t+k-j) \\
& - \sum_{j=k}^{n_{22}} c_{22}(j, u_1(t+k-1-j))u_2(t+k-1-j) \\
A_{11}(k) &= A_{11}(k-1) + \sum_{j=1}^k c_{11}(j, u_2(t)) - \sum_{j=1}^{k-1} c_{11}(j, u_2(t)) \\
A_{12}(k) &= A_{12}(k-1) + \sum_{j=1}^k c_{11}(j, u_1(t)) - \sum_{j=1}^{k-1} c_{12}(j, u_1(t)) \\
A_{21}(k) &= A_{21}(k-1) + \sum_{j=1}^k c_{21}(j, u_2(t)) - \sum_{j=1}^{k-1} c_{21}(j, u_2(t)) \\
A_{22}(k) &= A_{22}(k-1) + \sum_{j=1}^k c_{22}(j, u_1(t)) - \sum_{j=1}^{k-1} c_{22}(j, u_1(t))
\end{aligned} \tag{22}$$

with initials

$$\begin{aligned}
F_1(0) &= y_1(t), \quad F_2(0) = y_2(t), \quad A_{11}(0) = 0 \\
A_{12}(0) &= 0, \quad A_{21}(0) = 0, \quad A_{22}(0) = 0.
\end{aligned} \tag{23}$$

Denote

$$A = \begin{bmatrix} A_{11} & A_{12} \\ A_{21} & A_{22} \end{bmatrix} \quad F = \begin{bmatrix} F_1 \\ F_2 \end{bmatrix} \quad Y_0 = \begin{bmatrix} Y_{10} \\ Y_{20} \end{bmatrix} \quad U = \begin{bmatrix} u_1 \\ u_2 \end{bmatrix}. \tag{24}$$

Then the cost function (20) can be written as

$$G = (F(K) - Y_0 - A(K)U(t))^T (F(K) - Y_0 - A(K)U(t)). \tag{20'}$$

It can be seen from (22) that $A(K)$ depends on $U(K)$ being determined. Hence, minimization of G with respect to $U(K)$ is a nonlinear optimization problem.

In order to obtain an exact numerical solution of a nonlinear optimization, an iterative calculation is needed. For a real-time control, an on-line iterative calculation is not preferred. Hence, the necessity of implementing an on-line iterative calculation for achieving an exact numerical solution should be argued. It is known that the neurofuzzy model identified is a nominal model of the welding process. The unavoidable variations in the welding conditions such as the heat transfer condition cause the actual dynamics to differ from the nominal model. In this case, an exact numerical solution of the nonlinear optimization based on the nominal model may not exactly optimize the actual cost function. The error increases as the uncertainty of the process increases. For the welding process, the uncertainty which makes the closed-loop control necessary is substantial [8], [31]. Also, since there is no constraint on the change of the control action $U(t) - U(t-1)$, $U(t)$ determined based on the nonlinear optimization of (20) or (20') could significantly differ from $U(t-1)$. As a result, the control actions could be very energetic so that the resultant weld appearance is not smooth. Also, the large changes of the control actions and the significant difference between the actual dynamics and the nominal model could cause severe

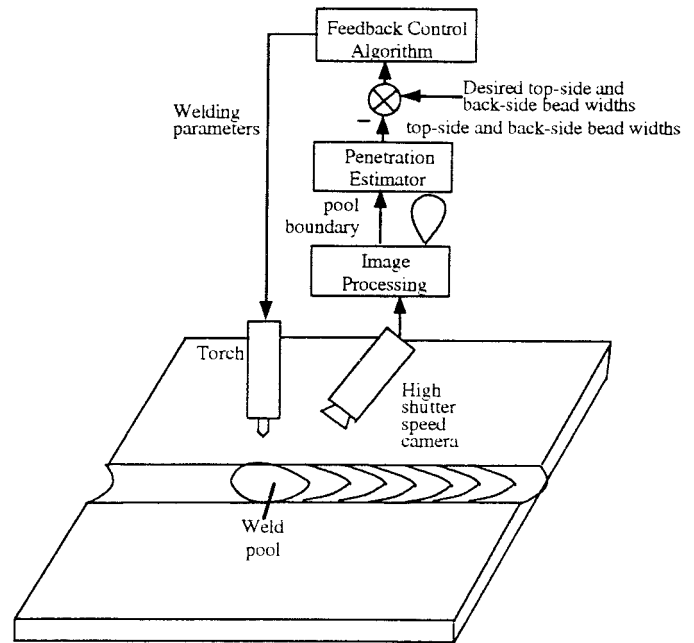


Fig. 13. Closed-loop control system.

errors between the predicted and actual outputs. The closed-loop system could be unstable. Hence, the following modified cost function is used:

$$\begin{aligned}
J &= (F(K) - Y_0 - A(K)U(t))^T (F(K) - Y_0 - A(K)U(t)) \\
& + (U(t) - U(t-1))^T \Lambda (U(t) - U(t-1))
\end{aligned} \tag{25}$$

where $\Lambda = \text{diag}(\lambda_1, \lambda_2)$ ($\lambda_1 \geq 0, \lambda_2 \geq 0$) are the weights.

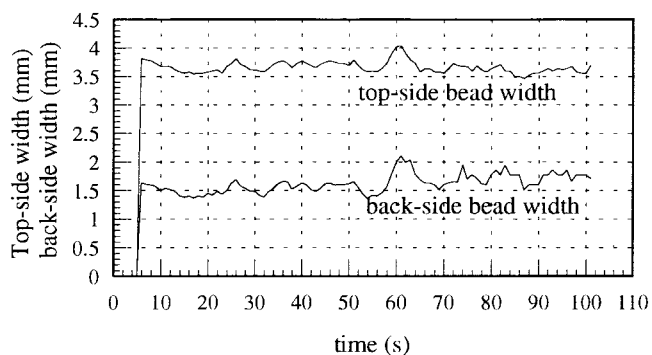
When the amplitudes of $U(t) - U(t-1)$ are not large, $c_{1i}(j, u_2(t))'s \dots$ can be approximated by $c_{1i}(j, u_2(t-1))'s \dots$ so that $A(K)$ can be calculated before the optimization. [The resultant accuracy in calculating $A(K)$ depends on the actual amplitudes of $U(t) - U(t-1)$.] Hence, the optimization becomes linear. The analytic solution is

$$\begin{aligned}
U(t) &= (A^T(K)A(K) + \Lambda)^{-1} (A^T(K)F(K) \\
& - A^T(K)Y_0 + \Lambda U(t-1)).
\end{aligned} \tag{26}$$

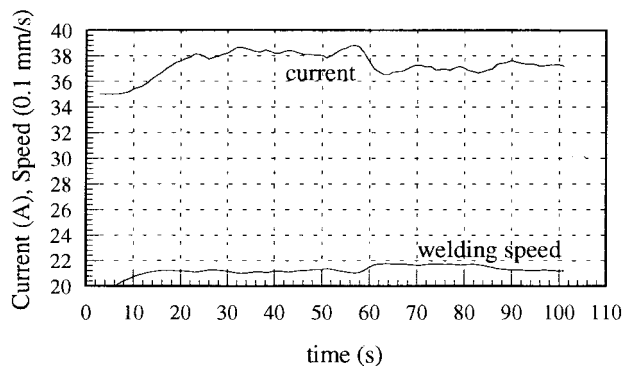
The values of the weights λ_1 and λ_2 can be determined based on their physical meaning in correlating the preferred changes of the control actions to the errors between the desired and measured outputs. In the developed system, $\lambda_1 = 10^2$ (mm/100 A)² is selected. This implies that an error of 1 mm in the predicted and desired top-side or back-side bead width has the same contribution to the cost function as $|u_1(t) - u_1(t-1)| = 0.1$, i.e., 10 A because the unit of in our control system is 100 A does. Similarly, $\lambda_2 = 10^2$ (mm²)² is selected.

VII. CLOSED-LOOP CONTROL EXPERIMENTATION

The developed closed-loop control system can be illustrated using the diagram in Fig. 13. In order to examine the robustness of the developed control system, uncertainties are emulated using a number of artificial disturbances in the closed-loop control experiments.



(a)



(b)

Fig. 14. Closed-loop control experiment of the top-side and back-side bead widths under step change in the rate of the shielding gas. (a) Outputs. (b) Control actions.

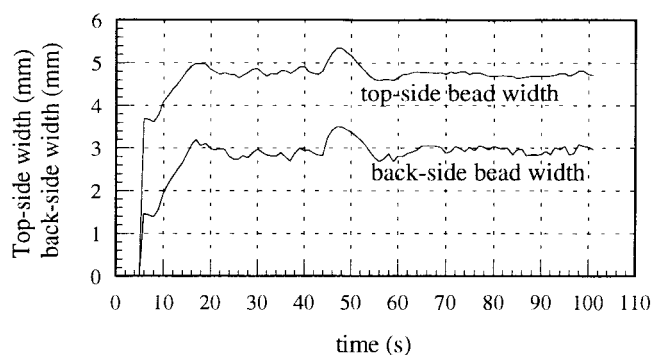
A. Experiment 1: Step Change of Rate of the Shielding Gas

In arc welding, the weld pool and electrode are prevented from being contaminated by the atmosphere by applying the shielding gas. In terms of circuit, the arc column can be regarded as a resistor in which the welding current flows and its resistance depends on both the arc length and shielding gas. The shielding gas (either the type or rate of the flow) has an influence on the welding arc, and, therefore, influences the weld pool.

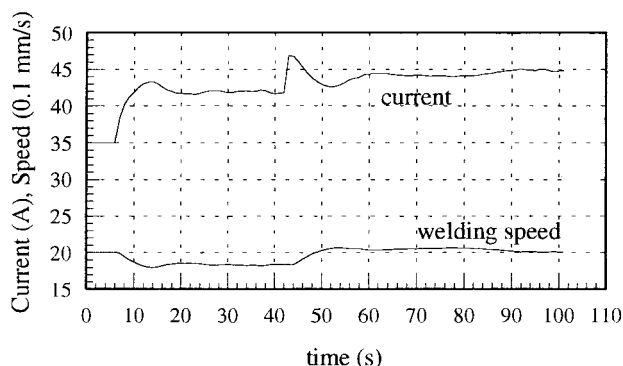
In this experiment, the initial rate of the argon flow was 27 l/min. At $t = 55$ s, the rate changes to 10 l/min (Fig. 14). As a result, both the top-side and back-side bead widths increase. As it can be observed in Fig. 14, by decreasing the welding current and increasing the welding speed, the closed-loop control system successfully eliminates the influence of the decrease in the rate of the argon flow.

B. Experiment 2: Current Disturbance

In this experiment, an artificial error between the actual and nominal values of the welding current is applied. During the first 42 s, no error exists between the actual and nominal values. From $t = 42$ s, the actual current is 5 A larger than the nominal value. Hence, both the top-side and back-side bead widths increases. As it can be seen in Fig. 15, the welding current and speed immediately decreases and increases, respectively, so that the outputs can be maintained at the desired levels again.



(a)



(b)

Fig. 15. Closed-loop control experiment of the top-side and back-side bead widths under step disturbance caused by the difference between the actual and nominal values of the welding current. (a) Outputs. (b) Control actions.

We notice that for advanced welding systems, such an error between the actual and nominal values of the welding current may not be frequently encountered. However, this artificial disturbance can change the dynamic model, which correlates the outputs to the nominal values of the welding parameters. Hence, a model perturbation is emulated.

C. Experiment 3: Speed Disturbance

In this experiment, an artificial error between the actual and nominal values of the welding speed is applied. During the first 52 s, no error exists between the actual and nominal values. However, after $t = 52$ s, the actual welding speed is 0.5 mm/s smaller than the nominal value. At $t = 52$ s, the welding current and speed are about 38 A and 2.2 mm/s, respectively. If no closed-loop correction is applied, 38 A welding current and 1.7 mm/s welding speed will increase the top-side and back-side bead widths by about 2 mm. Fig. 16 shows that this disturbance has been overcome by the closed-loop control system by simultaneously changing the welding current and welding speed.

Unlike the error between the actual and nominal values of the welding current, the error between the actual and nominal values of the welding speed can often be met in many applications. Hence, in addition to the emulation of the model perturbation, this experiment also shows that the developed closed-loop control system is robust with respect to the possible variation in the welding speed.

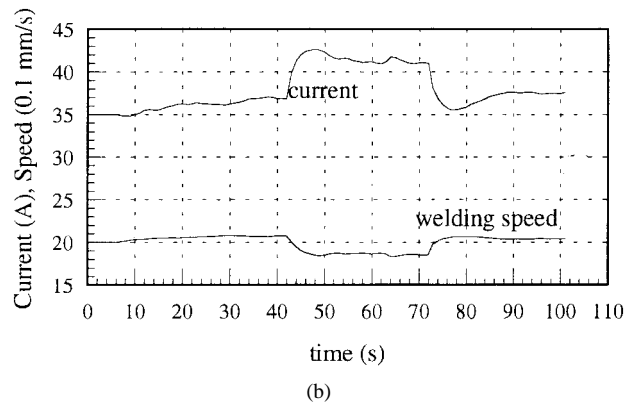
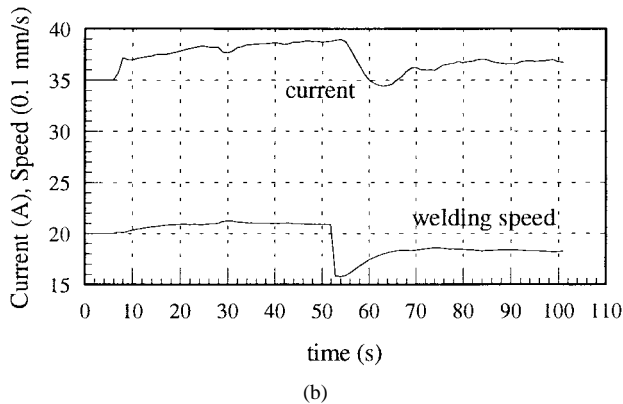
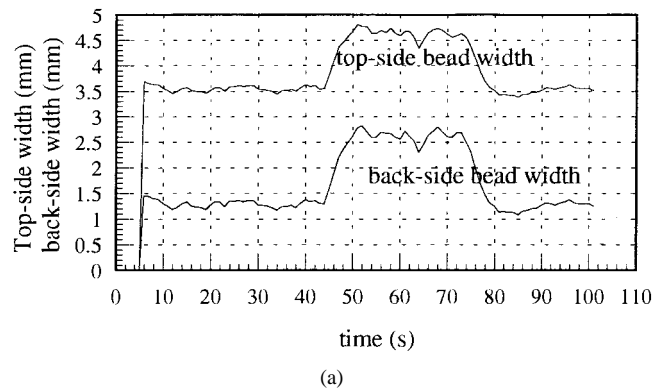
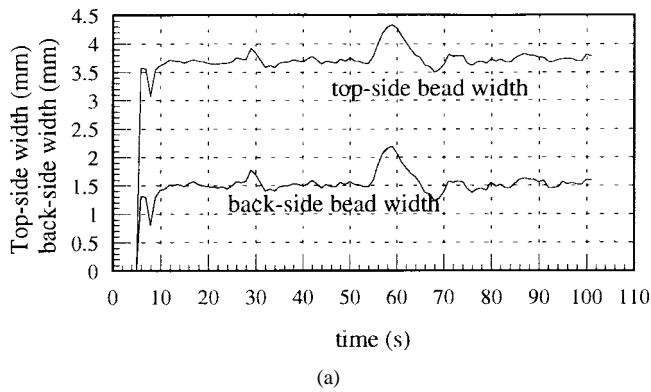


Fig. 16. Closed-loop control experiment of the top-side and back-side bead widths under step disturbance caused by the difference between the actual and nominal values of the welding speed. (a) Outputs. (b) Control actions.

Fig. 17. Closed-loop control experiment of the top-side and back-side bead widths in tracking varied set-points. (a) Outputs. (b) Control actions.

D. Experiment 4: Tracking Varying Set Points

Fig. 17 shows a closed-loop control experiment in tracking varied set-points. In general, the dynamic properties of the nonlinear process vary with the operating points. In order to track the varied set points, the operating points have to change. If a linear controller is used, the performance of the closed-loop control will in general not be guaranteed for different operating points. The welding experiment in Fig. 17 shows that the varied set points are well tracked. The similar results have also been observed in other experiments that tracked other varied set points.

VIII. CONCLUSIONS

The nonlinearity of the controlled process which has the welding current and speed as the inputs and back-side and top-side bead widths as the outputs is fundamental. The neurofuzzy model can describe the dynamic nonlinear process being controlled with sufficient accuracy. A neurofuzzy model based predictive algorithm has been developed to control the nonlinear welding process. The control experiments showed that the desired fusion state can be achieved by using the developed control system despite severe disturbances.

The developed system provides a solution to precise control of welding process. It is currently being used to weld aerospace materials. In applications where the requirement on the accuracy is relatively low and where the variations in the welding conditions are insignificant, other simpler control algorithms may also be used to ease the system design.

ACKNOWLEDGMENT

The authors would like to thank L. Li at the Center for Robotics and Manufacturing Systems Welding Research and Development Laboratory, University of Kentucky, Lexington, for his significant contributions in programming, data processing, and experimenting.

REFERENCES

- [1] A. R. Vorman and H. Brandt, "Feedback control of GTA welding using puddle width measurement," *Welding J.*, vol. 55, no. 9, pp. 742-749, 1976.
- [2] W. Chen and B. A. Chin, "Monitoring joint penetration using infrared sensing techniques," *Welding J.*, vol. 69, no. 4, pp. 181s-185s, 1990.
- [3] P. Banerjee, S. Govardhan, H. C. Wickle, H. Y. Liu, and B. A. Chin, "Infrared sensing for on-line weld geometry monitoring and control," *ASME J. Eng. Industry*, vol. 117, no. 3, pp. 323-330, 1995.
- [4] R. W. Richardson, D. A. Gutow, R. A. Anderson, and D. F. Farson, "Coaxial arc weld pool viewing for process monitoring and control," *Welding J.*, vol. 63, no. 3, pp. 43-50, 1984.
- [5] K. A. Pietrzak and S. M. Packer, "Vision-based weld pool width control," *ASME J. Eng. Industry*, vol. 116, no. 1, pp. 86-92, 1994.
- [6] J.-B. Song and D. E. Hardt, "Dynamic modeling and adaptive control of the gas metal arc welding process," *ASME J. Dynamic Syst., Meas., Contr.*, vol. 116, no. 3, pp. 405-413, 1994.
- [7] Y. M. Zhang, L. Wu, B. L. Walcott, and D. H. Chen, "Determining joint penetration in GTAW with vision sensing of weld-face geometry," *Welding J.*, vol. 72, no. 1, pp. 463s-469s, 1993.
- [8] Y. M. Zhang, R. Kovacevic, and L. Wu, "Dynamic analysis and identification of gas tungsten arc welding process for full penetration control," *ASME J. Eng. Industry*, vol. 118, no. 1, pp. 123-136, 1996.
- [9] Y. M. Zhang, R. Kovacevic, and L. Li, "Robust adaptive control of full penetration GTA welding," *IEEE Trans. Contr. Syst. Technol.*, vol. 4, pp. 394-403, July 1996.
- [10] R. Kovacevic, Y. M. Zhang, and R. Ruan, "Sensing and control of weld pool geometry for automated GTA welding," *ASME J. Eng. Industry*, vol. 117, no. 2, pp. 210-222, 1995.

- [11] T. Hoffman, "Real-time imaging for process control," *Advanced Mater. Processes*, vol. 140, no. 3, pp. 37–43, 1991.
- [12] R. Kovacevic and Y. M. Zhang, "Neurofuzzy model-based weld fusion state estimation," *IEEE Contr. Syst. Mag.*, vol. 17, no. 2, pp. 30–42, 1997.
- [13] *ASM Handbook—Welding, Brazing, and Soldering*. Materials Park, OH: Amer. Soc. Materials, 1993, vol. 6, pp. 30–35.
- [14] J. S. R. Jang and C. T. Sun, "Neuro-fuzzy logic modeling and control," *Proc. IEEE*, vol. 83, pp. 378–406, Mar. 1995.
- [15] E. H. Mamdani and S. Assilian, "An experiment in linguistic synthesis with a fuzzy logic controller," *Int. J. Mach. Studies*, vol. 7, no. 1, pp. 1–13, 1975.
- [16] R. Du, M. A. Elbestawi, and S. M. Wu, "Automated monitoring of manufacturing processes—Part 1: Monitoring methods," *ASME J. Eng. Industry*, vol. 117, no. 2, pp. 121–132, 1995.
- [17] T. J. Ko and D. W. Cho, "Tool wear monitoring in diamond turning by fuzzy pattern recognition," *ASME J. Eng. Industry*, vol. 116, no. 2, pp. 225–232, 1994.
- [18] S. B. Billatos and J. A. Webster, "Knowledge-based expert system for ballscrew grinding," *ASME J. Eng. Industry*, vol. 115, no. 2, pp. 239–235, 1993.
- [19] X. D. Fang, "Expert system-supported fuzzy diagnosis finish-turning process states," *Int. J. Mach. Tools Manuf.*, vol. 35, no. 6, pp. 913–924, 1995.
- [20] M. Brown and C. Harris, *Neurofuzzy Adaptive Modeling and Control*. Englewood Cliffs, NJ: Prentice-Hall, 1994.
- [21] K. Tanaka, M. Sano, and H. Watanabe, "Modeling and control of carbon monoxide concentration using a neuro-fuzzy technique," *IEEE Trans. Fuzzy Syst.*, vol. 3, pp. 271–279, Aug. 1995.
- [22] K. Hayashi, Y. Shimizu, Y. Dote, A. Takayama, and A. Hirako, "Neuro fuzzy transmission control for automobile with variable loads," *IEEE Trans. Contr. Syst. Technol.*, vol. 3, no. 1, pp. 49–53, Mar. 1995.
- [23] A. M. Sharaf and T. T. Lie, "Neuro-fuzzy hybrid power system stabilizer," *Elect. Power Syst. Res.*, vol. 30, no. 1, pp. 17–23, 1994.
- [24] O. S. Mesina and R. Langari, "Neuro-fuzzy system for tool condition monitoring in metal cutting," in *ASME Int. Mech. Eng. Congress Dynamic Syst. Contr.*, Chicago, IL, Nov. 1994, vol. 2, pp. 931–938.
- [25] T. Takagi and M. Sugeno, "Fuzzy identification of systems and its applications to modeling and control," *IEEE Trans. Syst., Man, Cybern.*, vol. 15, pp. 116–132, Jan./Feb. 1985.
- [26] D. B. Parker, "Optimal algorithms for adaptive networks: second order back propagation, second order direct propagation, and second order Hebbian learning," in *Proc. IEEE Int. Conf. Neural Networks*, San Diego, CA, Jan. 1987, pp. 593–600.
- [27] *Using NeuralWorks*. NeuralWare, Inc., Pittsburgh, PA, 1993.
- [28] S. Haykin, *Neural Networks: A Comprehensive Foundation*. New York: Macmillan College Publ., 1994.
- [29] D. W. Clarke, C. Mohtadi, and P. S. Tuffs, "Generalized predictive control-part 1: The basic algorithm," *Automatica*, vol. 23, pp. 137–148, 1987.
- [30] J. V. de Oliveira and J. M. Lemos, "Long-range predictive adaptive fuzzy relational control," *Fuzzy Sets Syst.*, vol. 70, no. 2/3, pp. 337–357, 1995.
- [31] K. C. Mills and B. J. Keene, "Factors affecting variable weld penetration," *Int. Mater. Rev.*, vol. 35, no. 4, pp. 185–216, 1990.



Yu M. Zhang (M'96–SM'97) received the B.S. and M.S. degrees in control engineering, and the Ph.D. degree in mechanical engineering, all from Harbin Institute of Technology (HIT), Harbin, China, in 1982, 1984, and 1990, respectively.

He joined the National Key Laboratory for Advanced Welding Production Technology at HIT, in 1984, as a Junior Lecturer, and was promoted to Full Professor in 1993. Since 1991 he has been with the Center for Robotics and Manufacturing Systems at the University of Kentucky, Lexington, KY, where he is currently supervising the Welding Research and Development Laboratory and the Applied Machine Vision Laboratory. He has authored and co-authored over 50 referred journal papers in welding, modeling, and control. His current research interest focuses on monitoring and control of welding and manufacturing processes and industrial applications.

Dr. Zhang is a senior member of the Society of Manufacturing Engineers (SME) and a member of the American Society of Mechanical Engineers (ASME) and American Welding Society (AWS). He received the 1995 Donald Julius Groen Prize from the Institution of Mechanical Engineers, U.K. for his paper published in the Institution's journal.



Radovan Kovacevic received the B.S. and M.S. degrees in mechanical engineering from the University of Belgrade, Yugoslavia, in 1969 and 1972, respectively, and the Ph.D. degree in mechanical engineering from the University of Montenegro, Podgorica, Yugoslavia, in 1978.

He is a Herman Brown Professor for Materials and Manufacturing Processes and Director of Laboratory for Manufacturing Processes and Systems at Southern Methodist University, Dallas, TX. He was Associate and Full Professor of mechanical engineering at the University of Kentucky, Lexington (1991–1997), an Associate Professor of mechanical engineering at Syracuse University, Syracuse, NY (1987–1990), and spent more than 16 years as part of the faculty at the University of Montenegro, Yugoslavia. He is an Honorary Consultant Professor at the Harbin Institute of Technology, Harbin, China. He was a Visiting Fulbright Scholar, Alexander von Humboldt Scholar (Germany), and Carl Duisberg Scholar (Germany). His research includes modeling, sensing and control of welding processes, abrasive waterjet processes and high-power laser beam processes, applied machine vision in quality control, and development of the rapid prototyping techniques. He holds two U.S. patents and has published more than 230 technical papers and five books.

Dr. Kovacevic received the Best Paper Award from the Institution of Mechanical Engineers, U.K., in 1995. He was the recipient of the 1997 American Welding Society Adams Memorial Membership Award. He is a Fellow of the Society of Manufacturing Engineers.